Supporting Information

Ultrafine Carbon Encapsulated NiRu Alloys as Bifunctional Electrocatalyst Boosting Overall-Water-Splitting: Morphological and Electronic Modulation through Minor Ru Alloying

Qifeng Yang[a], Peng Jin[b,*], Bing Liu[c], Liang Zhao[a], Jiahao Cai[a], Zhan Wei[b], Shouwei Zuo[c], Jing Zhang[c], Lai Feng[a,*]

[a]College of Energy, Soochow Institute for Energy and Materials InnovationS & Key Laboratory of Advanced Carbon Materials and Wearable Energy Technologies of Jiangsu Province, Soochow University, Suzhou 215006, China

[b]School of Materials Science and Engineering, Hebei University of Technology, Tianjin 300130, China

[c]Beijing Synchrotron Radiation Facility (BSRF), Institute of High Energy Physics of the Chinese Academy of Sciences, Beijing, 100049, China

Corresponding authors.

E-mail: fenglai@suda.edu.cn (L. Feng)

china.peng.jin@gmail.com (P. Jin)

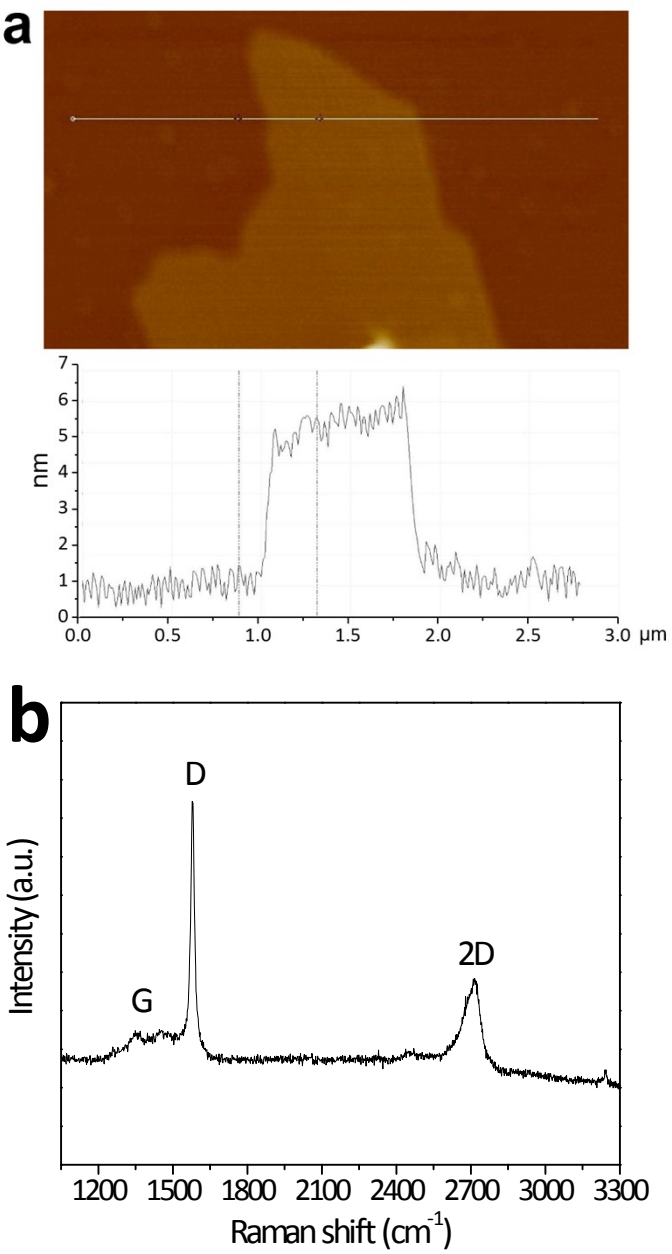

Figure S1. (a) AFM height image of graphene nanosheets and (b) their Raman spectrum obtained using λ_{ex}=514 nm.

The AFM image and corresponding height profile reveal that the graphene nanosheet has a thickness of ca. 5 nm, indicative of 7-10 graphene layers. The lateral size of graphene nanosheet is around a few micrometers. Besides, the Raman spectrum shows very weak G band at 1356 cm^{-1} and very strong D band at 1580 cm^{-1} along with evident 2D band at 2716 cm^{-1}. All these spectral feature reveal that the graphene nanosheets are less-defective.

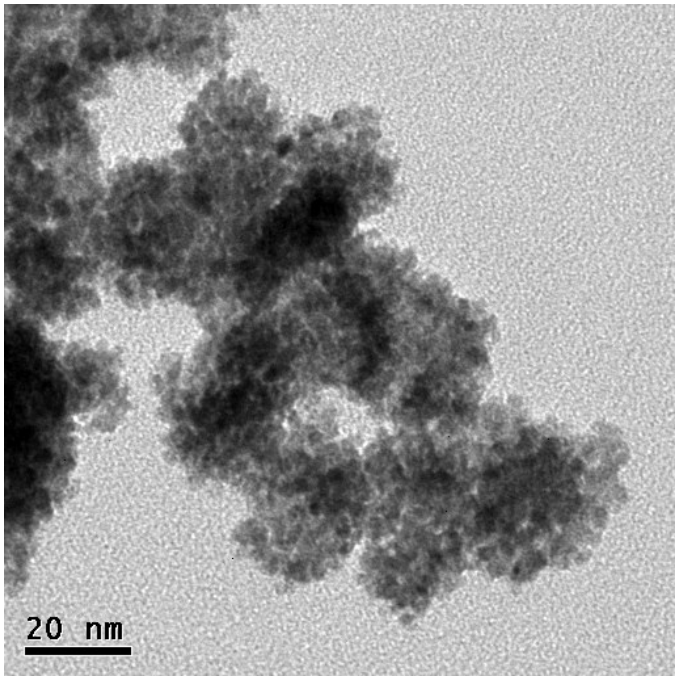

Figure S2. TEM image of nano-sized Ru NPs.

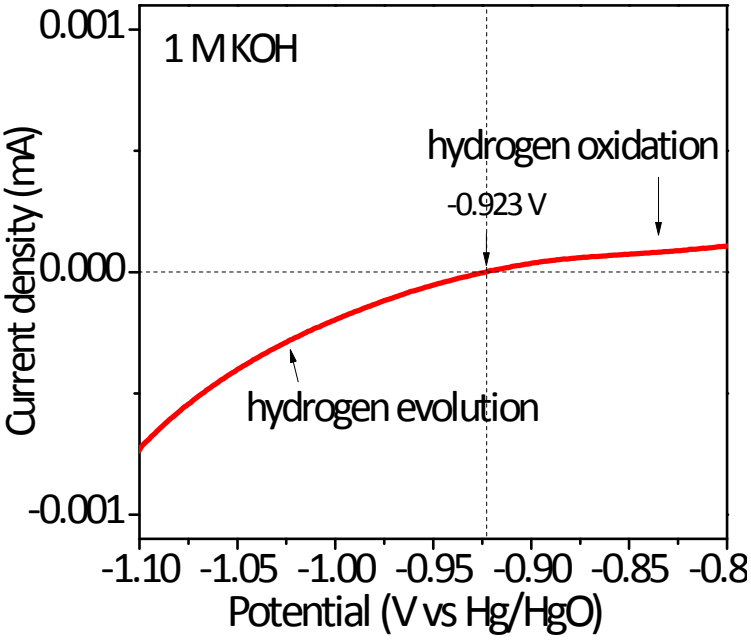

Figure S3. Calibration of reference electrode Hg/HgO in 1 M KOH.

The calibration of Hg/HgO electrode was performed in a standard three-electrode system with a Pt wire as the working and counter electrodes, and the Hg/HgO as the reference electrode. Electrolyte was pre-purged and saturated with high purity H_2. Linear scanning voltammetry (LSV) is then run at a scan rate of 0.5 mV s^{-1}, and the potential at which the current crossed zero is taken to be the thermodynamic potential for the hydrogen electrode reactions. For example, in 1 M KOH, the zero current point is at -0.923 V, so E (RHE) = E (Hg/HgO) + 0.923 V.

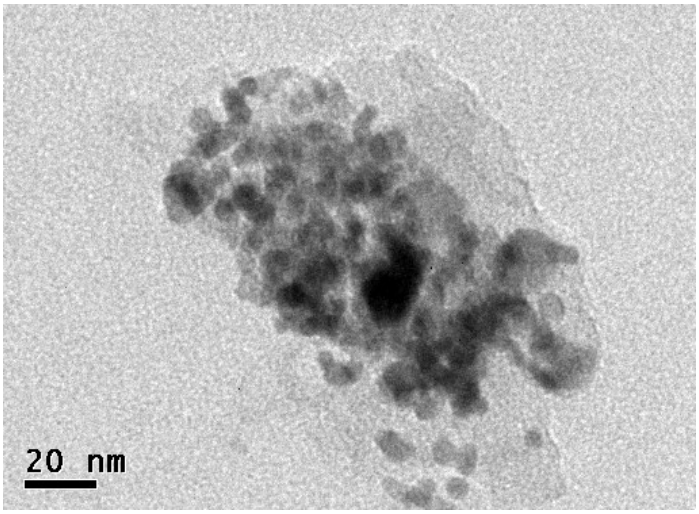

Figure S4. TEM image of $Ni_{0.6}Ru_{0.4}$@C NPs.

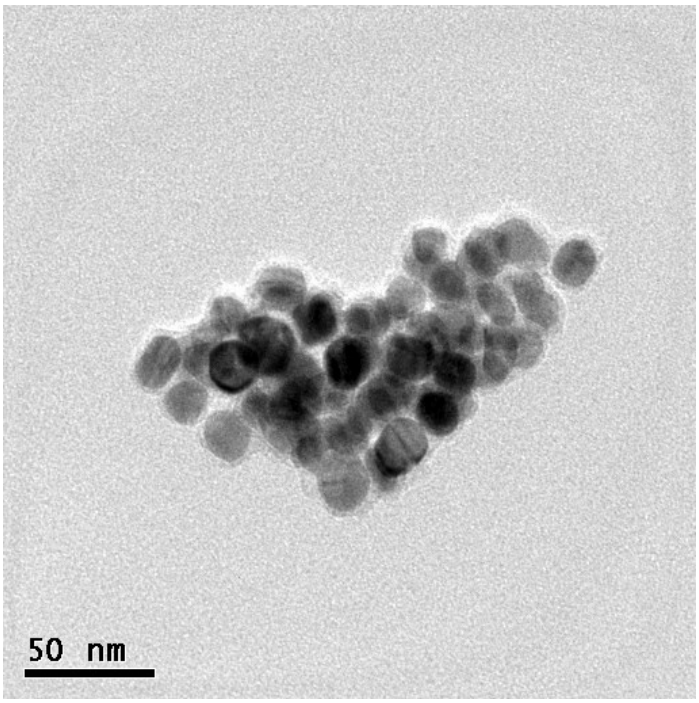

Figure S5. TEM image of Ni@C NPs.

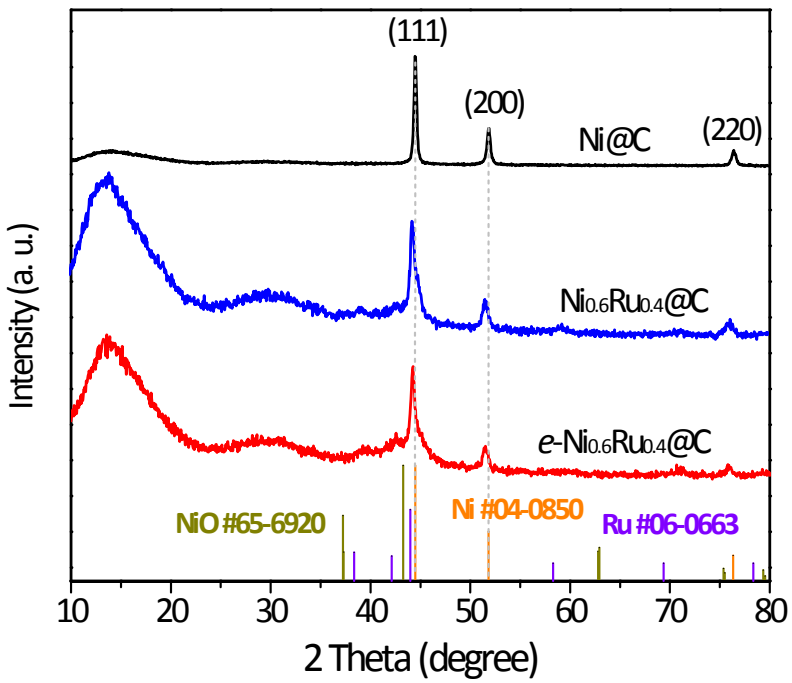

Figure S6. XRD spectra of *e*-$Ni_{0.6}Ru_{0.4}$@C, $Ni_{0.6}Ru_{0.4}$@C and Ni@C.

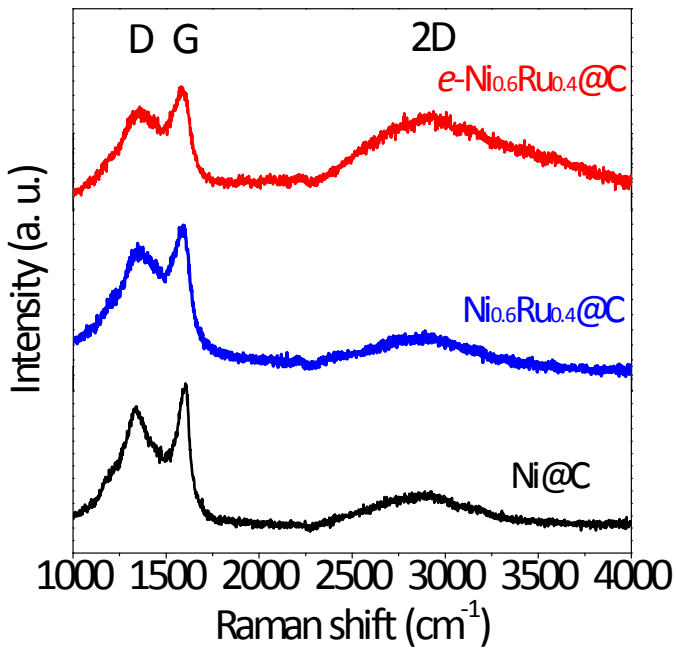

Figure S7. Raman spectra of *e*-$Ni_{0.6}Ru_{0.4}$@C, $Ni_{0.6}Ru_{0.4}$@C and Ni@C.

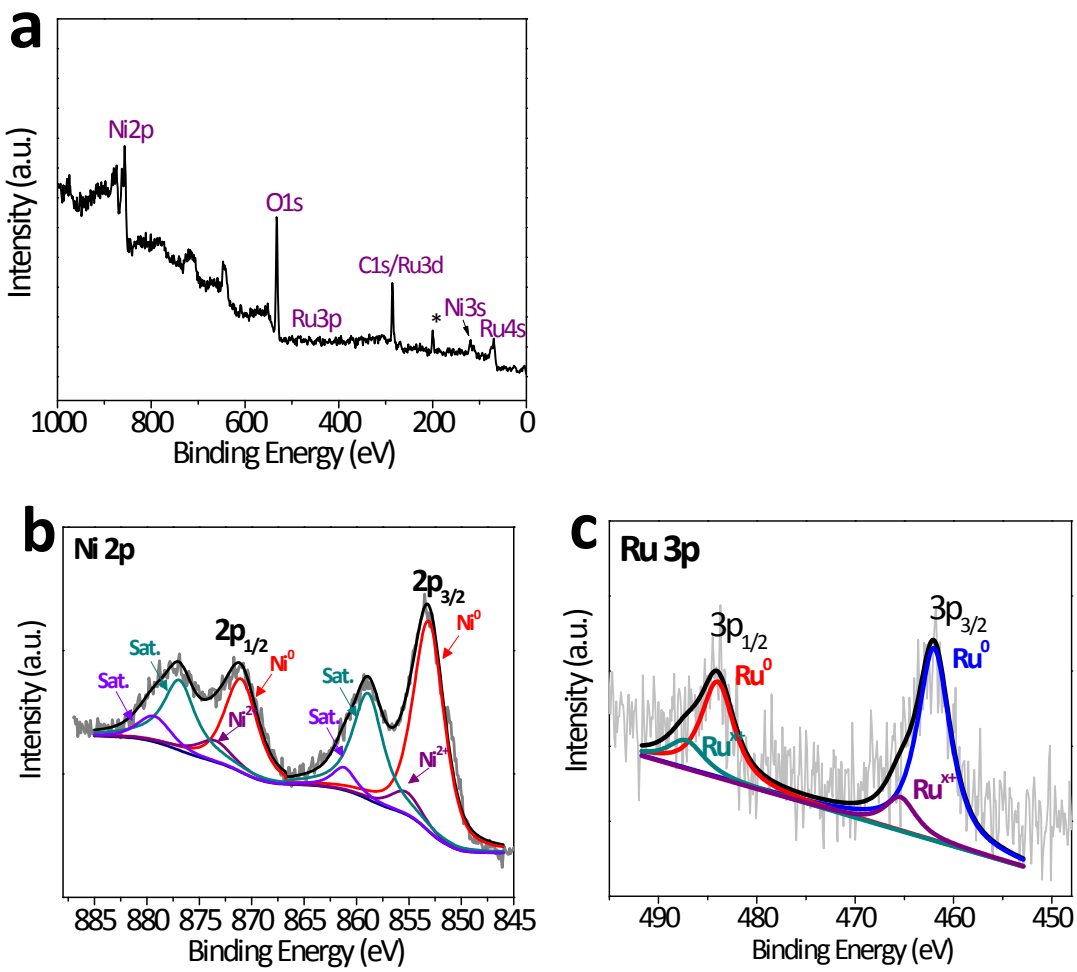

Figure S8. (a) XPS survey and (b) Ni 2p, (c) Ru 3p spectra of $Ni_{0.6}Ru_{0.4}$@C NPs.

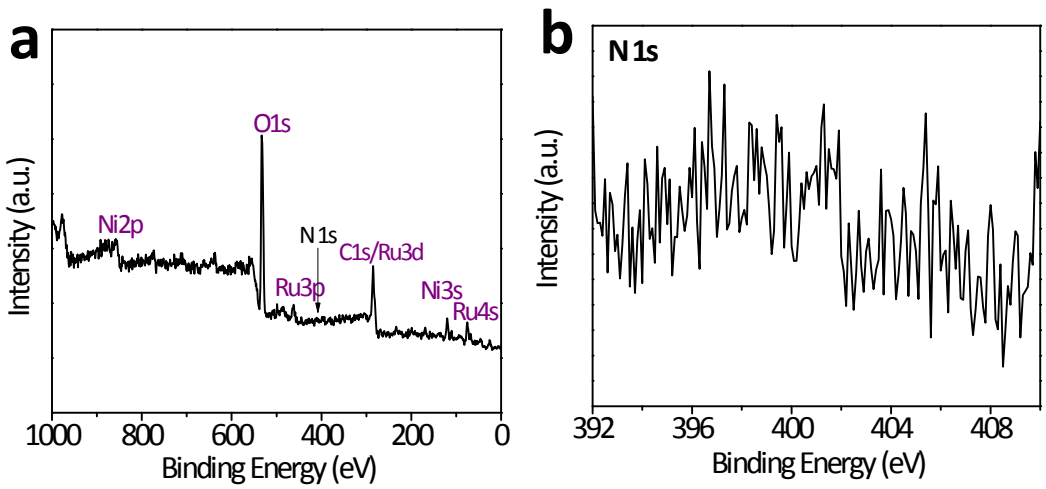

Figure S9. (a) XPS survey and (b) N1s spectra of *e*-$Ni_{0.6}Ru_{0.4}$@C NPs.

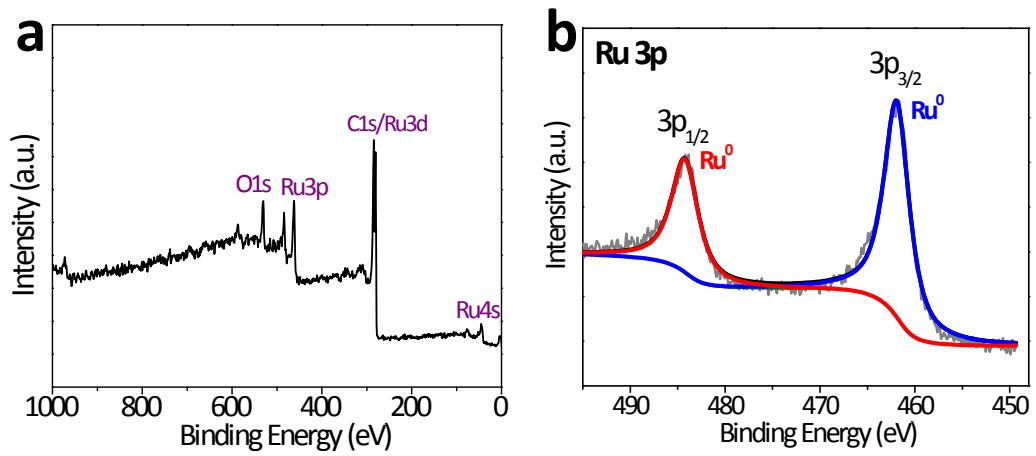

Figure S10. (a) XPS survey and (b) Ru 3p spectra of Ru NPs.

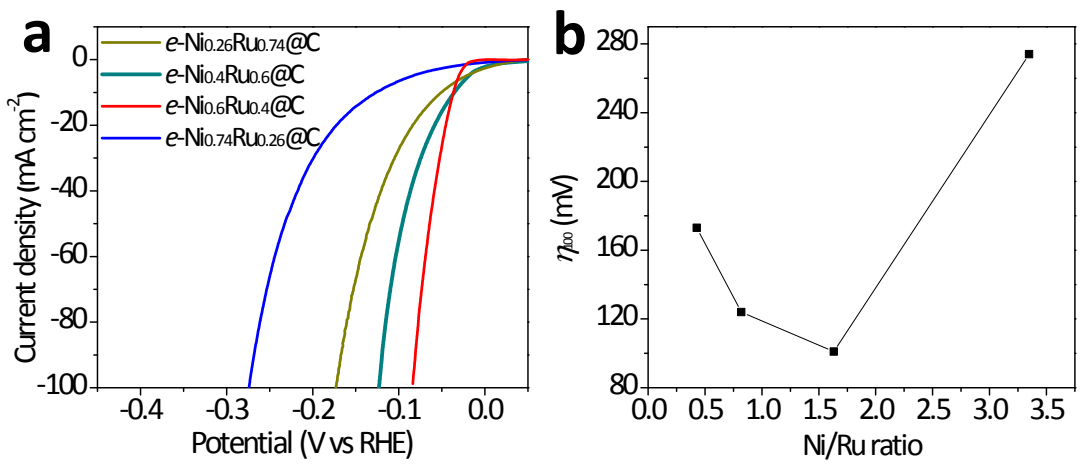

Figure S11. Electrochemical properties of the *e*-$Ni_{0.6}Ru_{0.4}$@C catalysts prepared from the $NiCl_2$ and $RuCl_3$ with different molar ratios. (a) HER polarisation curves (iR-corrected) for a scan rate of 1 mV·S^{-1} in 1 M KOH electrolyte. (b) Plot of the overpotential (η_{100}) at 100 mA/cm^{-2} as a function of Ni/Ru ratio.

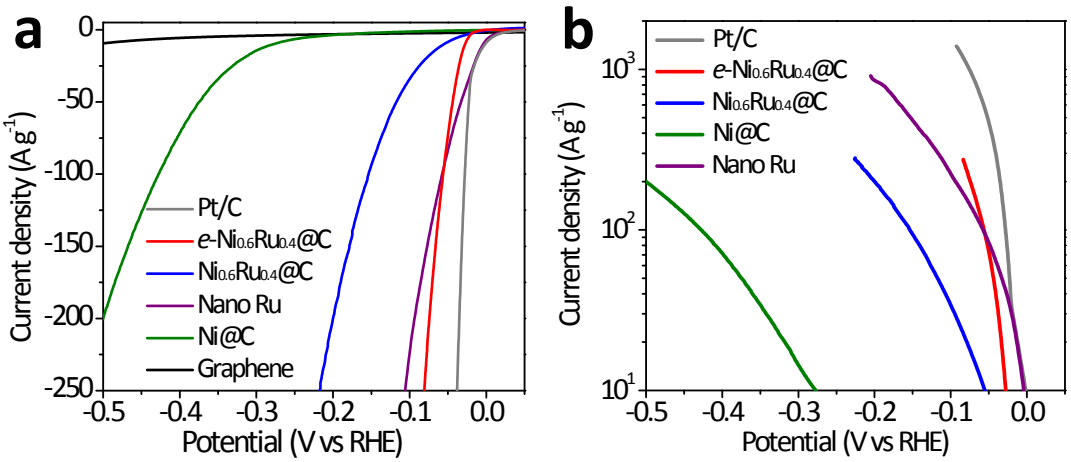

Figure S12. HER mass activities of various catalysts: (a,b) HER polarization curves measured in 1 M KOH with catalyst loading of 0.36 mg/cm^2, scan rate 5 mV/s and normalized with catalyst or Pt mass loading.

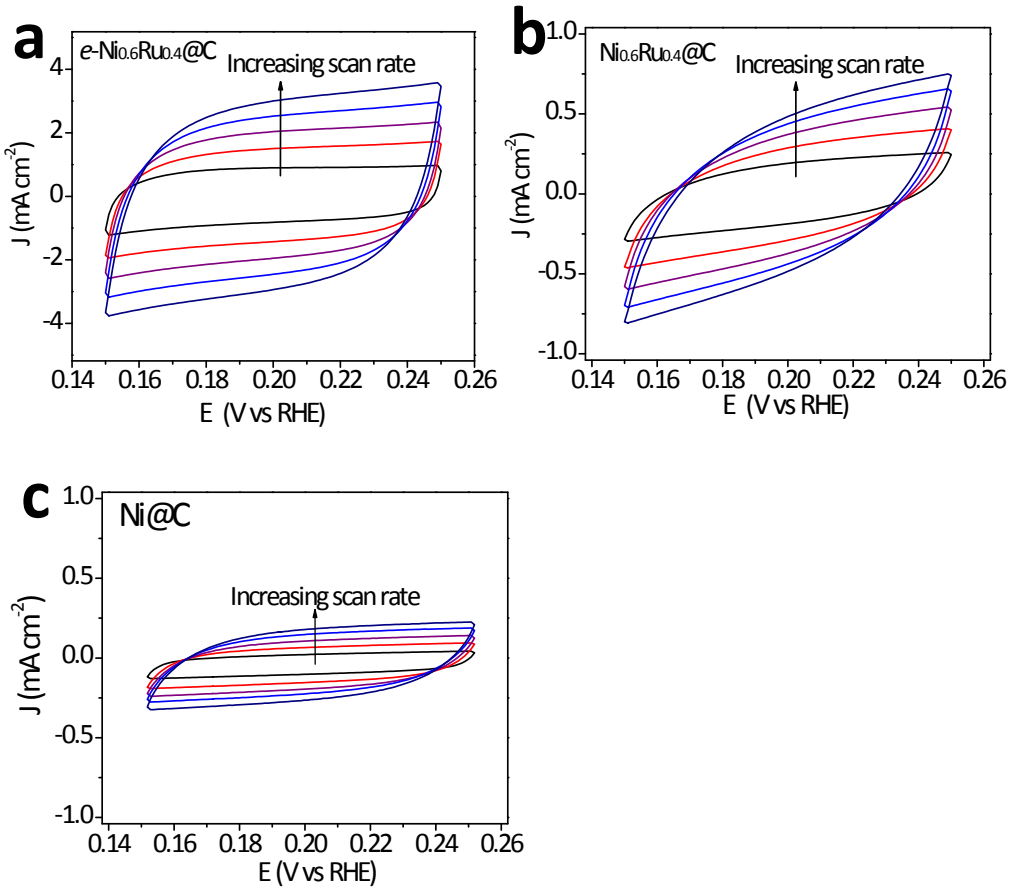

Figure S13. CV curves of (a) *e*-$Ni_{0.6}Ru_{0.4}$@C, (b) $Ni_{0.6}Ru_{0.4}$@C and (c) Ni@C with various scan rates.

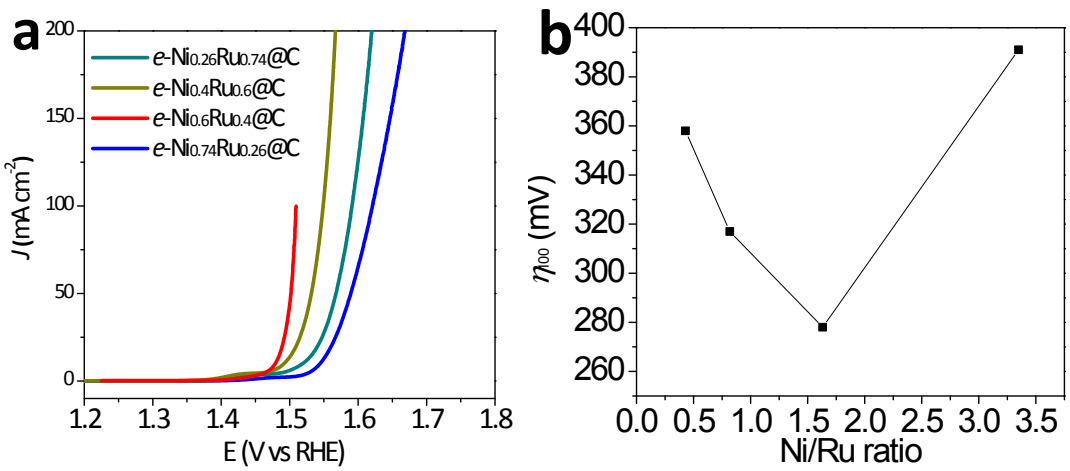

Figure S14. Electrochemical properties of the *e*-$Ni_{0.6}Ru_{0.4}$@C catalysts prepared from the $NiCl_2$ and $RuCl_3$ with different molar ratios. (a) OER polarisation curves (iR-corrected) for a scan rate of 1 mV·S^{-1} in 1 M KOH electrolyte. (b) Plot of the overpotential (η_{100}) at 100 mA/cm^{-2} as a function of Ni/Ru ratio.

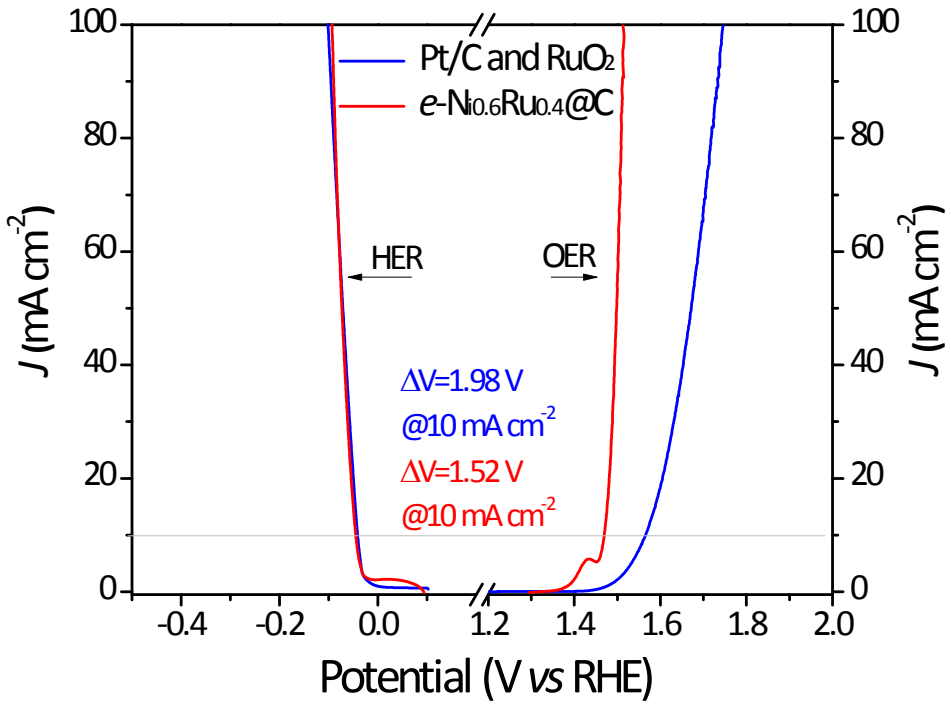

Figure S15. IR-corrected polarization curves of *e*-$Ni_{0.6}Ru_{0.4}$@C, Pt/C and RuO_2 for HER and OER, respectively, in 1 M KOH.

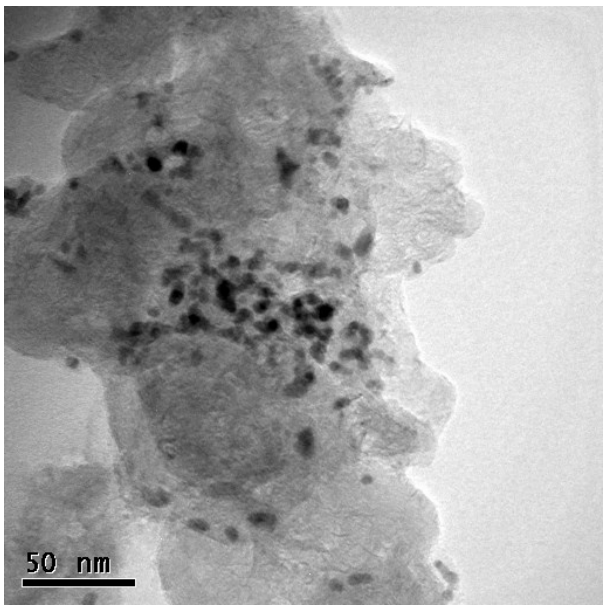

Figure S16. TEM image of the *e*-$Ni_{0.6}Ru_{0.4}$@C catalyst stripped off the carbon fiber substrate after the CP test.

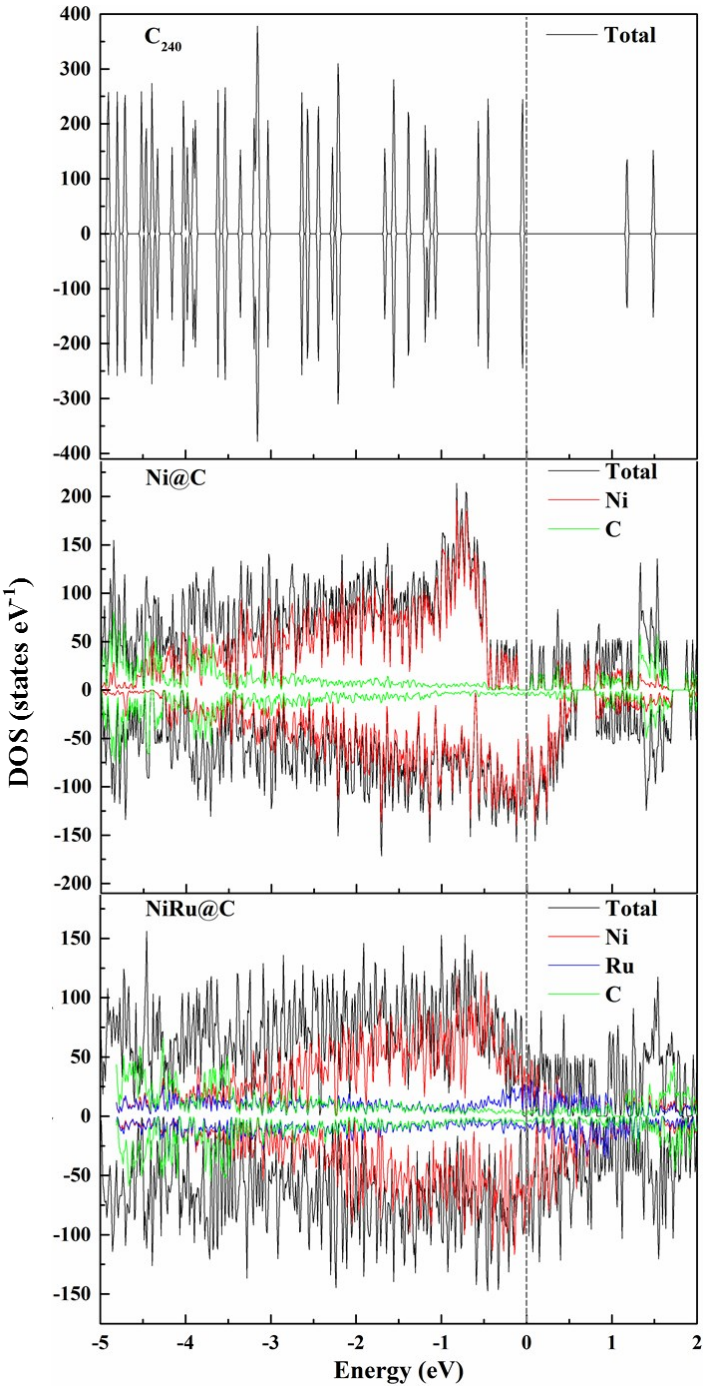

Figure S17. Density of states and partial density of states of the C_{240} carbon cage, $Ni_{55}@C_{240}$ and $Ni_{43}Ru_{12}@C_{240}$ models.

Table S1. Summary of the performances of the M@carbon based electrocatalysts for HER, OER and OWS in 1 M KOH.

Catalyst	η_{10} for HER (mV)	η_{10} for OER (mV)	η_{10} for OWS (V)	reference
NiRu@C	33	250	1.51/1.62 (η_{100})$^{a}_{ir}$	This work
$Co_{0.31}Mo_{1.69}C$/MXene/NC	75	---	---	1
Co@NPC-H	---	350	---	2
hcp-NiFe@NC	---	226	---	3
NiFe-N-CNT	250	270	1.58^{b}_{ir}	4
Ni QD@NC@rGO	133	265	1.563^{a}_{ir}	5
CoP@3D-NPC	203			6
OsP_2@NPC	90			7
Co/β-Mo_2C@N-CNT	170	356	1.64^{b}_{ir}	8
Ni/Mo_2C-NCNFs	133	288	1.64^{b}_{ir}	9
Co-NC@ Mo_2C	99	347	1.685^{a}_{ir}	10
Ni NP|Ni–N–C	147			11
FeP/NCNSs	205			12
B,N:Mo_2C@BCN	100	360 (η_{100})	$1.84^{b}(\eta_{100})_{ir}$	13
NiFe@C	195	214	1.575^{a}_{ir}	14
NiS@C	232			15
$MoSe_2$-NiSe@C	180			16
MoP@C	49			17
Mo_2C-MoP NPC/CFP-800	146			18
Co-Mo_2C@NCNT	186	337	1.628^{c}	19
Fe-Ni@NC-CNTs	202	274	$1.98^{b}(\eta_{145})_{ir}$	20
FLNPC@MoP-NC/MoP-C/CC	69			21
MoP/NPG	115			22
VC@NCNT	159			23
Y–S Ni–Co-Se/CFP	250	300		24
CoPS@NPS-C	191	320		25
CoNP@C	58			26
S-CoWP@(S,N)-C	67	280	1.65_{ir}	27
Mo_2C@NC	60			28
$NiCo_2O_4$@C	109	267	1.608^{b}	29

[a]Catalyst-modified carbon fiber was used as electrode.
[b]Catalyst-modified nickel foam was used as electrode.
[c]Catalyst-modified Ti plate was used as electrode.
$_{ir}$ refers to the ir-corrected cell voltage for overall water splitting.

References in **Table S1**.

[1].X. Wu, S. Zhou, Z. Wang, J. Liu, W. Pei, P. Yang, J. Zhao, and J. Qiu, *Adv. Energy Mater.* 2019, **9**, 1901333.

[2].Y.-N. Hou, Z. Zhao, H. Zhang, C. Zhao, X. Liu, Y. Tang, Z. Gao, X. Wang, J. Qiu, *Carbon* 2019, **144**, 492-499.

[3].C. Wang, H. Yang, Y. Zhang, and Q. Wang, *Angew. Chem. Int. Ed.* 2019, **58**, 6099 –6103.

[4].W. Wan, S. Wei, J. Li, C. A. Triana, Y. Zhou and G. R. Patzke, *J. Mater. Chem. A,* 2019, **7**, 15145-15144.

[5].Z. Chen, H. Xu, Y. Ha, X. Li, M. Liu and R. Wu, *Appl. Catal. B: Environ.,* 2019, **250**, 213-223.

[6].S. Yang, L. Chen, W. Wei, X. Lv and J. Xie, *Appl. Surf. Sci.,* 2019, **476**, 749-756.

[7].S. Chakrabartty, B. K. Barman and C. Retna Raj, *Chem Commun (Camb),* 2019, **55**, 4399-4402.

[8].T. Ouyang, Y. Q. Ye, C. Y. Wu, K. Xiao and Z. Q. Liu, *Angew. Chem. Int. Ed.*, 2019, **58**, 4923-4928.

[9].M. Li, Y. Zhu, H. Wang, C. Wang, N. Pinna and X. Lu, *Adv. Energy Mater.*, 2019, **9**, 1803185.

[10]. Q. Liang, H. Jin, Z. Wang, Y. Xiong, S. Yuan, X. Zeng, D. He and S. Mu, *Nano Energy,* 2019, **57**, 746-752.

[11]. C. Lei, Y. Wang, Y. Hou, P. Liu, J. Yang, T. Zhang, X. Zhuang, M. Chen, B. Yang, L. Lei, C. Yuan, M. Qiu and X. Feng, *Energy Environ. Sci.,* 2019, **12**, 149-156.

[12]. Y. Yu, Z. Peng, M. Asif, H. Wang, W. Wang, Z. Wu, Z. Wang, X. Qiu, H. Tan and H. Liu, *ACS Sustain. Chem. Eng.,* 2018, **6**, 11587-11594.

[13]. M. A. Anjum, M. H. Lee and J. S. Lee, *ACS Catal.,* 2018, **8**, 8296-8305.

[14]. W. Park, I. Kim, I. Oh, J.C. Kim and D.W. Kim, *J. Catal.,* 2018, **366**, 266-274.

[15]. J. Zhang, Y. Wang, J. Cui, J. Wu, X. Shu, C. Yu, H. Bai, M. Zhai, Y. Qin, H. Zheng, Y. Zhu, Y. Zhang and Y. Wu, *Int. J. Hydrogen Energy*, 2018, **43**, 16061-16067.

[16]. C. Liu, K. Wang, X. Zheng, X. Liu, Q. Liang and Z. Chen, *Carbon*, 2018, **139**, 1-9.

[17]. G. Li, Y. Sun, J. Rao, J. Wu, A. Kumar, Q. Xu, C. Fu, E. Liu, G. R. Blake, P.Werner, B. Shao, K. Liu, S. Parkin, X. Liu, M. Fahlman, S.-C. Liou, G. Auffermann, J. Zhang, C. Felser and X. Feng, *Adv. Energy Mater.,* 2018, **8**, 1801258.

[18]. T. Liu, H. Liu, X. Wu, Y. Niu, B. Feng, W. Li, W. Hu and C. Li, *Electrochim. Acta*, 2018, **280**, 710-716.

[19]. L. Ai, J. Su, M. Wang and J. Jiang, *ACS Sustain. Chem. Eng.*, 2018, **6**, 9912-9920.

[20]. X. Zhao, P. Pachfule, S. Li, J. R. Simke, J. Schmidt and A. Thomas, *Angew. Chem. Int. Ed.*, 2018, **57**, 8921-8926.

[21]. B. Liu, H. Li, B. Cao, J. Jiang, R. Gao and J. Zhang, *Adv. Funct. Mater.,* 2018, **28**, 1801527.

[22]. K. Lan, X. Wang, H. Yang, K. Iqbal, Y. Zhu, P. Jiang, Y. Tang, Y. Yang, W. Gao, R. Li, *ChemElectroChem,* 2018, **5**, 2256-2262.

[23]. L. Cao, N. Zhang, L. Feng, J. Huang, Y. Feng, W. Li, D. Yang and Q. Liu, *Nanoscale*, 2018, **10**, 14272-14279.

[24]. K. Ao, J. Dong, C. Fan, D. Wang, Y. Cai, D. Li, F. Huang and Q. Wei, *ACS Sustain. Chem. Eng.,* 2018, **6**, 10952-10959.

[25]. Y. Hu, F. Li, Y. Long, H. Yang, L. Gao, X. Long, H. Hu, N. Xu, J. Jin and J. Ma, *J. Mater. Chem. A,* 2018, **6**, 10433-10440.

[26]. Q. Jin, B. Ren, D. Li, H. Cui and C. Wang, Nano Energy, 2018, **49**, 14-20.

[27]. Q. Weng, C. R. Grice, W. Meng, L. Guan, F. Xu, Y. Yu, C. Wang, D. Zhao and Y. Yan, *ACS Energy Letters,* 2018, **3**, 1434.

[28]. J. Chi, W. Gao, W. Lin, B. Dong, J. Qin, Z. Liu, B. Liu, Y. Chai and C. Liu, *J. Catal.,* 2018, **360**, 9-19.

[29]. J. Deng, H. Zhang, Y. Zhang, P. Luo, L. Liu and Y. Wang, *J. Power Sources,* 2018, **372**, 46-53.

Table S2. ICP-AES analysis results of *e*-Ni_xRu_y@C, Ni_xRu_y@C catalysts.

Catalyst	Ni wt%	Ru wt%	Fe wt%	Ni/Ru molar ratio
e-$Ni_{0.26}Ru_{0.74}$@C	31.9	45.4	2.7	1.2
e-$Ni_{0.4}Ru_{0.6}$@C	49.1	31.0	2.0	2.7
e-$Ni_{0.6}Ru_{0.4}$@C	42.5	20.6	1.6	3.6
$Ni_{0.6}Ru_{0.4}$@C	63.5	19.8	0	5.6
e-$Ni_{0.74}Ru_{0.26}$@C	65.9	13.0	4.1	8.7

Note: ICP analysis revealed that only trace Fe species remained in *e*-Ni_xRu_y@C catalysts after the etching process probably due to the interaction between Fe^{2+} and OA. As the exhedral graphitic carbon shell provides the catalytic sites, the trace endohedral Fe species may provide negligible influence on the electronic state of the graphitic carbon shell[1] and hence is not further considered in the discussions.

Reference

[1].W. Wan, S. Wei, J. Li, C. A. Triana, Y. Zhou and G. R. Patzke, *J. Mater. Chem. A,* 2019, **7**, 15145-15144.

Table S3. Impedance spectra fitting results for the HER of *e*-$Ni_{0.6}Ru_{0.4}$@C, $Ni_{0.6}Ru_{0.4}$@C and Ni@C in 1 M KOH.

Samples	R_S (Ω)	R_c (Ω)	CPE1-T (10^{-3}S.sec^n/cm^2)	CPE1-P (S.sec^n/cm^2)	R_t (Ω)	CPE2-T (10^{-3}S.sec^n/cm^2)	CPE2-P (S.sec^n/cm^2)
e-$Ni_{0.6}Ru_{0.4}$@C	2.1	0.1	11.6	0.83	1.1	10.8	0.86
$Ni_{0.6}Ru_{0.4}$@C	2.3	0.2	23.4	0.64	3.5	3.8	0.92
Ni@C	1.8	0.9	52.6	0.52	22.3	3.8	0.97

Table S4. Summary of the catalytic performances of the NiRu-based nanostructures for HER, OER and OWS in 1 M KOH.

Catalyst	η_{10} for HER(mV)	η_{10} for OER (mV)	η_{10} for OWS (V)	reference
e-$Ni_{0.6}Ru_{0.4}$@C	33	250	1.51/1.62 (η_{100})[a]ir	This work
Ni_2Ru_2 SNs	40	230	1.6	1
Ni@Ru HNS		320		2
$Ni_{43}Ru_{57}$ nanoalloy	41 (H_2SO_4)			3
Ru_3Ni_3 NAs	39	304	1.52	4
Ru/Ni_3N–Ni	53	200	1.55 (η_{20})	5

References in **Table S4**

[1].J. Ding, Q. Shao, Y. Feng, X. Huang, *Nano Energy,* 2018, **47**, 1-7.

[2].Hwang, H.; Kwon, T.; Kim, H. Y.; Park, J.; Oh, A.; Kim, B.; Baik, H.; Joo, S. H.; Lee, K, *Small,* 2018, 14 ,1702353.

[3].Zhang, C.; Liu, Y.; Chang, Y.; Lu, Y.; Zhao, S.; Xu, D.; Dai, Z.; Han, M.; Bao, J., *ACS Appl Mater Interfaces,* 2017, **9**, 17326-17336.

[4].Yang, J.; Shao, Q.; Huang, B.; Sun, M.; Huang, X, *iScience,* 2019, **11**, 492-504.

[5].Liu, Z.; Zha, M.; Wang, Q.; Hu, G.; Feng, L, *Chem Commun,* 2020, **56**, 2352-2355.